Laser-produced L-series x-ray spectra*

P. G. Burkhalter and D. J. Nagel
Naval Research Laboratory, Washington, D. C. 20375

Robert D. Cowan
University of California, Los Alamos Scientific Laboratory, Los Alamos, New Mexico 87544

(Received 26 September 1974)

The Ne I resonance transitions were measured with sufficient precision to extend the spectroscopy of the Ne I isoelectronic sequence to $Z = 40$. *Ab initio* atomic-structure calculations and isoelectronic extrapolations are in agreement with the measured values. Atomic-structure calculations were used to interpret the Na- and Mg-like satellite lines in the $2p$-$3s$ and $2p$-$3d$ regions in Se and Zr. The interpretation of the L-series satellites may prove important for future plasma diagnostics.

I. INTRODUCTION

X rays from highly stripped ions are produced in the hot plasmas formed at the focus of high-power lasers. Identification of x-ray emission from transitions to the K shell in the atomic number range[1] $10 \leq Z \leq 22$ and M-shell transitions in the range[2,3] $50 \leq Z \leq 68$ have recently been completed. The purpose of the present work with the laser-plasma source and crystal spectrographs is to determine the ionization stages in the hot plasmas from measurement of the L-shell x-ray emission in the range $29 \leq Z \leq 40$. This provides part of the basis for the use of L spectra from medium-Z elements for plasma diagnostics. The ultraviolet (uv) emissions produced by vacuum-spark sources and measured with grating spectrographs were classified by Edlén and Tyrén[4,5] as the Ne I isoelectronic sequence in the 1930's at Uppsala for the range $19 \leq Z \leq 27$ and extended to the ionization state Zn XXI by Feldman *et al.*[6] at Goddard. Here, we observe resonance-emission transitions in the Ne I sequence and nearby ionization states. The identifications are made by a combination of isoelectronic sequence extrapolations plus *ab initio* atomic-structure calculations. The energy calibrations have sufficient precision for atomic spectroscopy purposes and this work extends the Ne I isoelectronic sequence to $Z = 40$.

II. EXPERIMENTAL

The 100-GW Nd:glass laser system[7] at the Naval Research Laboratory produced a 1.06-μm-wavelength laser beam that was focused by means of a 74-cm-focal-length lens onto the surface of solid slab targets. The mode-locked oscillator coupled with a Fabry-Perot etalon generated a main pulse with a width of 900 psec. A low temperature plasma condition was generated with a small prepulse 0.7 nsec ahead of the main pulse. X-ray spectra were generated in targets of Zn, Ge, Se, KBr, and Zr in the 10–20 J on-target power level. A flat-crystal Bragg spectrograph was used with Kodak (No-screen) x-ray film to collect spectra in the 1–3-keV range. The Zn and Ge spectra were obtained with a potassium acid phthlate (KAP) crystal ($2d = 26.6$ Å). An ammonium dihydrogen phosphate (ADP) crystal ($2d = 10.640$ Å) was used to obtain the Se, Br, and Zr spectra. Each spectrum was obtainable with a single laser shot except the Zr spectrum which was obtained with two shots of ~10 J on target. Calibration spectra were obtained with shots on NaCl, Mg, Al, Si, and S targets. The hydrogen- and helium-like resonance lines from these elements had a sufficient energy range to span the unknown x-ray lines for the higher-Z targets. Calibration energies used were from the tabulations of Kelly and Palumbo.[8] Portions of the unknown x-ray spectra from the high-Z elements were calibrated with spectra from different calibration elements. The spectra from adjacent calibration elements overlapped sufficiently that an experimental precision of ±1–2 eV or about ±0.1% was obtained in the determination of transition energies in this work.

III. RESULTS

A. Ne-like spectra

The x-ray spectrum obtained with a Zn target[9] in the energy range of 1050–1600 eV consisted of complex arrays of x-ray multiplets from F- and O-like ionization stages in addition to distinct lines from simple multiplet structure for the Ne I sequence.[6] The resonance lines in the Ne I sequence correspond to transitions from the $2p^5 3s$, $2p^5 3d$, $2s2p^6 3p$, and $2p^5 4s$, $4d$ configurations to the ground state $2s^2 2p^6\ ^1S_0$. The isolated $2p$-$3s$ doublet and intense lines from $2p$-$3d$ and $2p$-$4d$ transitions in Ne I are particularly distinct lines that characterize L-series x-ray spectra from transition ele-

TABLE I. Experimental values for transitions in the Ne I isoelectronic sequence.

Zn XXI				Br XXVI		
Expt. energy (eV)	Expt. wave length (Å)	Previous λ values (Å) and classification[a]		Expt. energy (eV)	Expt. wave length (Å)	Classification in *jj* coupling
1057	11.73	11.76	$^1S_0$-$^3P_1$	1542	8.04	$2p^6$-[$2p^5(^2P_{3/2})$, $3s$]$_1$
1079	11.49	11.51	$^1S_0$-$^1P_1$	1589	7.80	$2p^6$-[$2p^5(^2P_{1/2})$, $3s$]$_1$
1148	10.80	10.80	$^1S_0$-$^3P_1$	1665	7.45	$2p^6$-[$2p^5(^2P_{3/2})$, $3d(^2D_{3/2})$]$_1$
1162	10.67	10.67	$^1S_0$-$^3D_1$	1684	7.36	$2p^6$-[$2p^5(^2P_{3/2})$, $3d(^2D_{5/2})$]$_1$
1185	10.46	10.47	$^1S_0$-$^1P_1$	1727	7.18	$2p^6$-[$2p^5(^2P_{1/2})$, $3d(^2D_{3/2})$]$_1$
1262	9.82		$^1S_0$-$^3P_1$	1817	6.82	$2s^22p^6$-[$2s2p^63p(^2P_{1/2})$]$_1$
1269	9.77	9.77	$^1S_0$-$^1P_1$	1831	6.77	$2s^22p^6$-[$2s2p^63p(^2P_{3/2})$]$_1$
1420	8.73		$^1S_0$-$^3P_0$	2088	5.94	$2p^6$-$2p^54s$
1434	8.65		$^1S_0$-$^1P_1$	2104	5.89	$2p^6$-$2p^54s$
1466	8.46		$^1S_0$-$^3D_1$	2144	5.78	$2p^6$-$2p^54d$
1488	8.33		$^1S_0$-$^3P_1$	2189	5.66	$2p^6$-$2p^54d$

[a] Values from Feldman *et al.* (Ref. 6).

ments. In the laser-produced Zn spectrum the Ne- and F-like line arrays have roughly equal intensities. The experimentally determined energies for the Ne-like transitions in Zn XXI have been tabulated in Table I in both x-ray energy and wavelength using a conversion factor of 12 398 eV/Å. Previous wavelength values with *LS* coupling classification are listed for comparison. There is excellent agreement for the $2p$-$3d$ and $2s$-$3p$ transitions. The laser-produced values for the first two transitions listed ($2p$-$3s$) might not have as high an experimental accuracy as other experimental values reported in this work because these two transitions occur at somewhat lower energies than the lowest calibration energies for $1s^2$-$1s2p$ He-like lines in Na.

The energy determinations for the Ne I transitions in Br XXVI are listed in Table I. The Br spectrum was similar to the Se spectrum that will be discussed.

The Ge spectrum obtained at the 10-J laser power level is shown in Fig. 1. The most distinct lines in this spectrum belong to the Ne-like isoelectronic sequence in Ge XXIII. The identified energy ranges for various transitions in Ne- and F-like spectra presented in this figure were obtained from

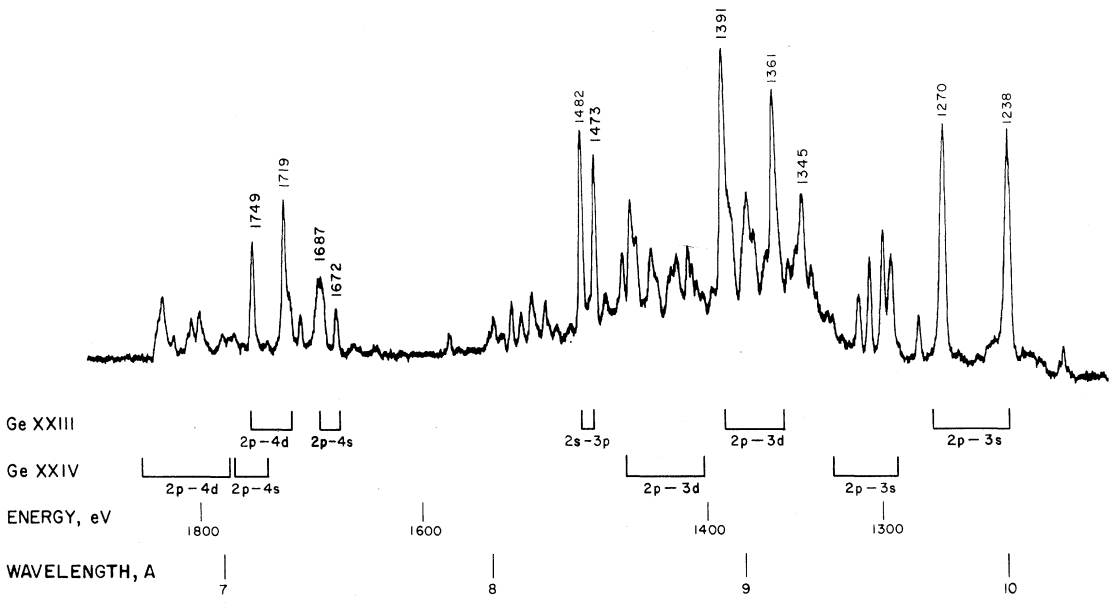

FIG. 1. Laser-produced x-ray spectrum for Ge with 10 J on target. The energy regions for the indicated transitions in Ne-like Ge XXIII and F-like Ge XXIV were obtained by extrapolation from published uv measurements. Prominent lines in the Ne I isoelectronic sequence are labeled with x-ray energy values above the spectrum.

extrapolation of vacuum spark data.[8] The $2s$-$3p$ inner-shell transitions are distinct in Ge XXIII which was not the case in Zn because of overlap with $2p$-$3d$ transitions in O-like Zn XXIII. Also found in the Ge spectra are Na- and Mg-like transitions appearing as satellite structure around the $2p$-$3d$ and $2p$-$3s$ lines in Ge XXIII, which indicate the presence of lower ionization stages.

Proceeding up the periodic table to Se the laser-produced spectra shown in Fig. 2 become nearly devoid of F-like ionization states and the Se spectrum is a Ne-like pattern with intense satellite structure. Atomic-structure calculations were performed by one of us (R. D. C.) using a previously described computer program[10] to compare with the Ne-like transition energies and also to identify the satellite structure. The calculated energies are indicated below the Se spectrum in Fig. 2 for the Ne-like transitions in Se XXV and also for the satellite transitions that will be discussed later.

The Zr spectrum shown in Fig. 3 contains distinct Ne-like lines and intense Na- and Mg-like satellite lines. The calculated values for these ionization stages have been plotted in the figure.

The experimentally determined energies for the Ne-like transitions for Ge XXIII, Se XXV, and Zr XXXI have been tabulated together with calculated values for the Ne-like transitions to the $n=3$ levels in Table II. The transitions for this Z range are best represented in jj coupling and are so classified in the table. The agreement between experimental and theoretical wavelength values is within the ±0.1% experimental precision for all the transitions except for two in Se for which the agreement is within 0.2%.

The Ne I-like L-series x-ray transitions were found to form linear extrapolations with published vacuum-spark produced uv values[8] in a Moseley plot as shown in Fig. 4. In this figure the square root of the transition energies was plotted as a function of Z and joined by straight lines. The deviations of the laser-produced values are within 2 eV of the linear extrapolations of the published uv data except for three transitions in Zr which are 0.5% larger than the extrapolated values. These differences in Zr amounted to 12 eV for the $2p^6$-$2p^5(^2P_{1/2})3s$ and both $2s$-$3p$ transitions. The near linearity for the x-ray energies for highly

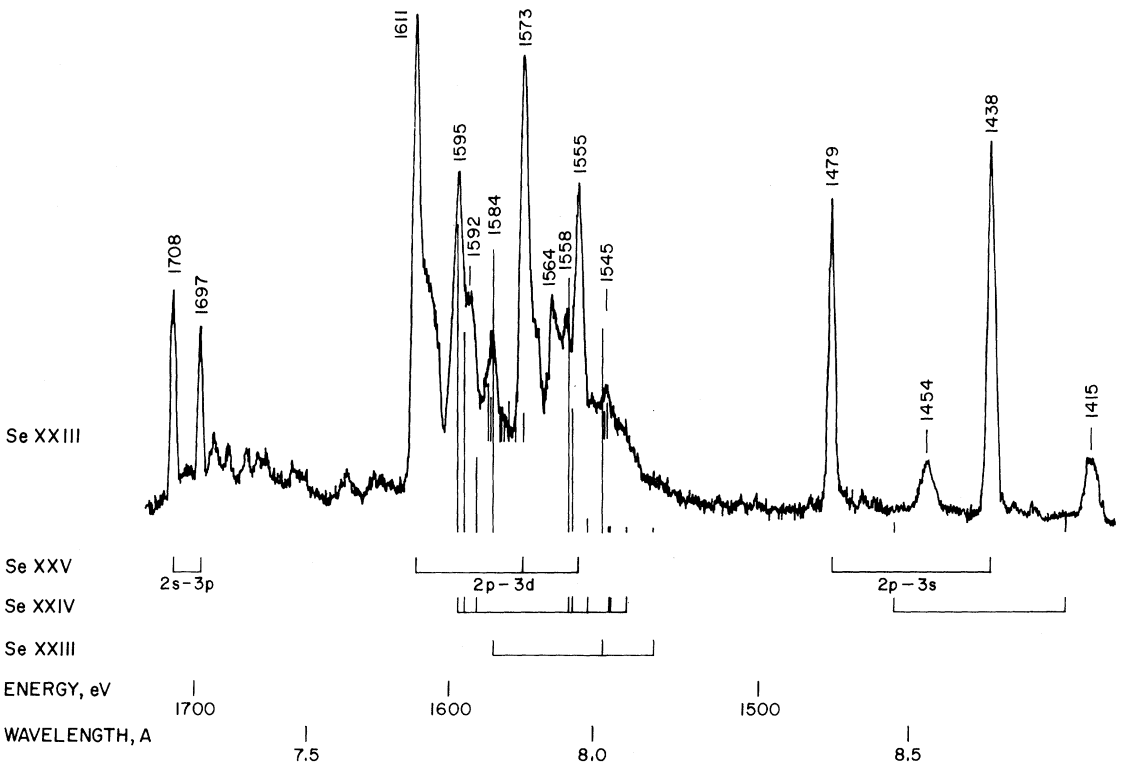

FIG. 2. Laser-produced spectrum for Se. Transition energies and relative oscillator strengths for Ne-like Se XXV and Na- and Mg-like satellites obtained by atomic structure calculations are indicated as vertical lines.

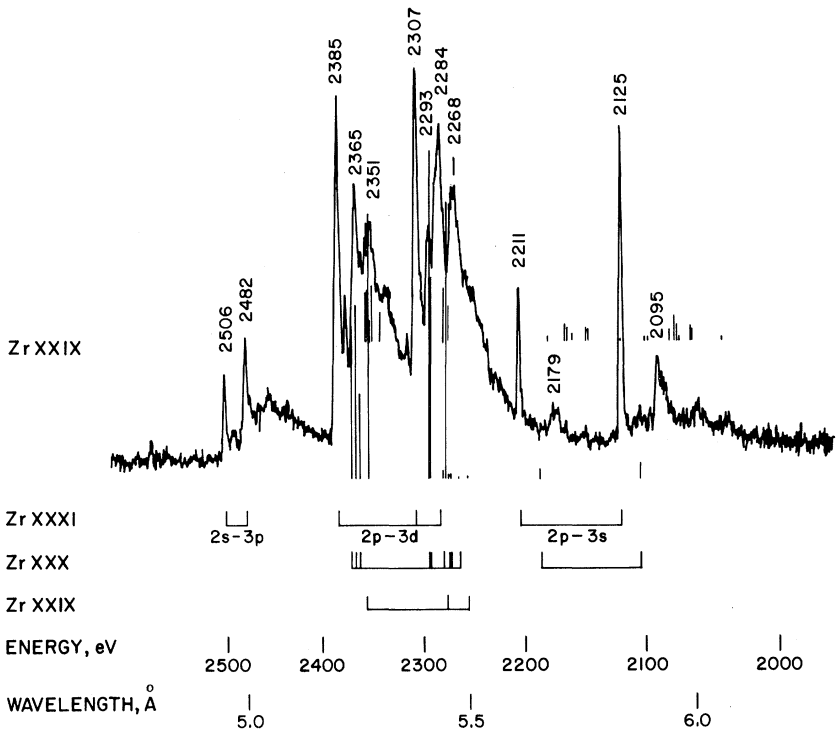

FIG. 3. Laser-produced spectrum for Zr and atomic-structure calculations.

TABLE II. Experimental and calculated values for transitions in the Ne I isoelectronic sequence.

Element	Expt. energy (eV)	Expt. wave length (Å)	Expt. int.	Calc. wave length (Å)	*gf*	Classification in *jj* coupling
Ge XXIII	1238	10.01	100	10.010	0.10	$2p^6$-$[2p^5(^2P_{3/2}), 3s]_1$
	1270	9.76	90	9.764	0.07	-$[2p^5(^2P_{1/2}), 3s]_1$
	1345	9.22	30	9.216	0.01	-$[2p^5(^2P_{3/2}), 3d(^2D_{3/2})]_1$
	1361	9.11	90	9.109	1.2	-$[2p^5(^2P_{3/2}), 3d(^2D_{5/2})]_1$
	1391	8.91	100	8.913	2.2	-$[2p^5(^2P_{1/2}), 3d(^2D_{3/2})]_1$
	1473	8.42	50	8.415	0.12	$2s^22p^6$-$[2s2p^63p(^2P_{1/2})]_1$
	1482	8.37	60	8.362	0.51	-$[2s2p^63p(^2P_{3/2})]_1$
	1672	7.42				$2p^6$-$2p^54s$
	1687	7.35				$2p^6$-$2p^54s$
	1719	7.21				$2p^6$-$2p^54d$
	1749	7.09				$2p^6$-$2p^54d$
Se XXV	1438	8.62	90	8.618	0.10	$2p^6$-$[2p^5$-$(^2P_{3/2}), 3s]_1$
	1479	8.38	70	8.380	0.07	-$[2p^5(^2P_{1/2}), 3s]_1$
	1555	7.97	40	7.965	0.01	-$[2p^5(^2P_{3/2}), 3d(^2D_{3/2})]_1$
	1573	7.88	90	7.874	1.4	-$[2p^5(^2P_{3/2}), 3d(^2D_{5/2})]_1$
	1611	7.70	100	7.688	2.1	-$[2p^5(^2P_{1/2}), 3d(^2D_{3/2})]_1$
	1697	7.31	20	7.295	0.14	$2s^22p^6$-$[2s2p^63p(^2P_{1/2})]_1$
	1708	7.26	30	7.244	0.51	-$[2s2p^63p(^2P_{3/2})]_1$
Zr XXXI	2125	5.83	70	5.832	0.10	$2p^6$-$[2p^5(^2P_{3/2}), 3s]_1$
	2211	5.61	40	5.612	0.07	-$[2p^5(^2P_{1/2}), 3s]_1$
	2284	5.43	30	5.433	0.00	-$[2p^5(^2P_{3/2}), 3d(^2D_{3/2})]_1$
	2307	5.37	90	5.373	1.8	-$[2p^5(^2P_{3/2}), 3d(^2D_{5/2})]_1$
	2385	5.20	100	5.203	1.8	-$[2p^5(^2P_{1/2}), 3d(^2D_{3/2})]_1$
	2482	5.00	20	4.998	0.18	$2s^22p^6$-$[2s2p^63p(^2P_{1/2})]_1$
	2506	4.95	20	4.957	0.52	-$[2s, 2p^63p(^2P_{3/2})]_1$

stripped atoms in a Moseley plot provides a simple and valuable method to identify x-ray transitions in higher-Z elements as laser power levels increase in the future.

To pursue the Ne sequence much further up the periodic table would require a higher laser power density than used in this work. The Zr spectrum was collected at the 10-J on-target level. The laser pulse was focused to a spot size on the target of <100-μm diameter. This was confirmed by an x-ray pinhole photograph of a Zr target shown in Fig. 5. A uniform x-ray hot spot is produced at the target surface with a measured 100-μm-diam area. Therefore a laser power density of at least about 10^{14} W/cm^2 is required to excite Ne-like transitions in Zr. The small size of the plasma allows collection of high resolution x-ray spectra in a slitless spectrograph.

B. Satellite transitions

Low-intensity complex structures that are so-called satellite transitions to the Ne I resonance lines have been observed in both vacuum-spark and solar spectra; however, a detailed interpretation as to the origin of the satellite structure has not been reported. Parkinson[11] measured energies of the weak satellite structure in a high-resolution Fe solar spectrum as have Feldman and Cohen[12] for Fe XVI satellites to the $2p$-$3s$ transitions in a vacuum-spark Fe spectrum. Also Feldman and Cohen[13] have measured and classified the two $2p^6 3s$-$2p^5 3s^2$ Na I satellites for Ti XII through Cu XIX. These were identifiable because their energy spacings are the same as between the two parent $2p^6$-$2p^5 3s$ lines in Ne-like transitions. The laser-produced Se and Zr x-ray spectra have strong satellite line structure while weak satellite structure is also observable in the Zn and Ge spectra. The most intense satellite lines would be expected to have ground-state configurations containing $n=3$ shell electrons. Atomic-structure calculations were made for $2p$-$3s$ and $2p$-$3d$ transitions with either $3s$, $3p$, or $3d$ electrons in the lower configuration to interpret the satellite lines in the Se and Zr spectra. In the Ge spectrum a portion of the satellite structure in the $2p$-$3s$ region is overlapped by the Ne I line at 1238 eV as seen in Fig. 1; however, the $2p^6 3s$-$2p^5 3s^2(^2P_{3/2})$ line is observed at 1215 ± 1.5 eV and agrees with the linear extrapolation of published data.[13]

Atomic-structure calculations were made for the transitions $2p^6 3s$-$2p^5 3s3d$ in Na-like Se XXIV and $2p^6 3s^2$-$2p^5 3s^2 3d$ in Mg-like Se XXIII to identify the intense satellites in the $2p$-$3d$ region. The calculated values were shifted by 0.013 Å to larger wavelengths to obtain correspondence with the observed satellite pattern. The calculated energy values are indicated for the corresponding ionization stage below the spectrum in Fig. 2 and the calculated relative oscillator strengths (gf values) for these particular satellites are plotted as vertical lines from the base of the spectrum. Examination of the Se spectrum reveals that most of the distinct lines in the $2p$-$3d$ region are accounted for by the above satellite transitions plus the three intense Ne-like lines. The line groupings at 1595, 1592, and 1558 eV are Na-like having an additional $3s$ electron in the ground configuration. The line at 1564 appears to be unaccounted for by these transitions. The lines at 1584 and 1545 eV correspond to satellite energies for two $3s$ electrons in Mg-like Se XXIII.

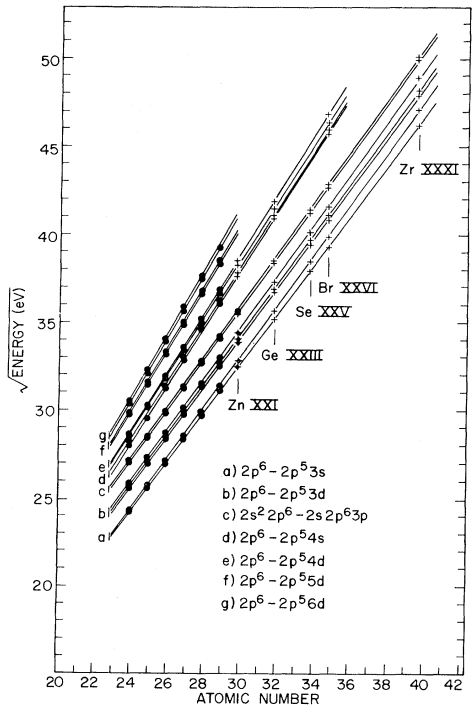

FIG. 4. Moseley plot for Ne I isoelectronic sequence. Solid dots, published measurements; crosses, our laser-produced values.

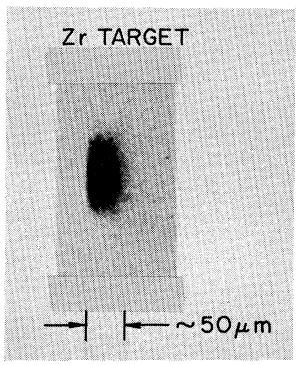

FIG. 5. 1–3-keV x-ray pinhole picture of a Zr target observed at 90° to the laser axis. The laser beam was incident from the right.

However, the L-series satellite peaks are complex because substitution of $3p$ or $3d$ electrons instead of $3s$ electrons can produce overlapping multiplet structure. While the theory predicts only a few $3s$ satellite peaks, substitution of $3p$ electrons yields complex multiplet structure with several hundred transitions. A few of the most intense $3p$ satellites in Se XXIII are illustrated by the vertical lines in the center of the Se spectrum which are plotted at a somewhat elevated intensity level. This explains why the satellite lines are broader than the Ne-like parent lines. The tailing towards lower energy seen on the Ne resonance lines (especially the 1611-eV line) is believed to be satellite structure due to the presence of additional electrons having $n>3$.

In the $2p$-$3s$ region for Se there are two groups of satellites at 1454 and 1415 eV that have an energy spacing that agrees with the calculated spacings between the two $2p^6 3s$-$2p^5 3s^2$ transitions in Na-like Se XXIV. However, there is discrepancy between the calculated and experimental satellite values. The satellite-energy separation agrees within 2 eV with the energy difference for the $2p$-$3s$ Ne-like lines. These satellites are broad as they have overlapping structure with satellites from configurations containing $3p$ electrons, as will be illustrated in the Zr spectrum.

The calculated energies of the $2p^6 3s$-$2p^5 3s 3d$ transitions in Na-like Zr XXX and $2p^6 3s$-$2p^5 3s 3d$ in Mg-like Zr XXIX have been plotted (unnormalized) in Fig. 3 together with the calculated oscillator strengths. The lines at 2365 and 2293 eV are Na-like while lines at 2351 and 2268 eV are Mg-like. Substitution of $3p$ electrons instead of $3s$ in the Mg-like transitions that are plotted at an elevated intensity demonstrate that the satellite lines are clusters of overlapping multiplets. Again the line clusters with distinct peaks at 2179 and 2095 eV have spacings equal to the calculated spacings and agree with the energy separation between the $2p$-$3s$ Ne-like transitions within 2 eV. Other weaker satellite clusters are observed in the $2p$-$3s$ region and the Mg-like satellite calculations with $3p$ electrons partially account for the satellite pattern. The use of an ethylenediamine-d-tartrate (EDDT) ($2d=8.808$ Å) or graphite crystal ($2d=6.74$ Å) would achieve higher resolution in the $2p$-$3s$ regions for Se and Zr, respectively; and thereby provide better separation of the satellite lines stages. The identification of satellite transitions is important because the measurement of satellite-to-parent intensity ratios have potential value for plasma diagnostics. The $2p^6 3s$-$2p^5 3s^2$ Na-like satellites appear to be the most readily distinguishable satellite lines. However, to obtain the intensity of the individual satellite lines ones should use the peak heights at 2179 and 2095 eV rather than the integrated satellite group.

C. Intensities

The experimental intensities listed for the Ne-like transitions in Table II have been corrected for absorption of the 1-mil Be window used as a light-tight cover for the x-ray film, for the x-ray crystal responses, and for the film-density effects. The Ge, Se, and Zr spectra in figures 1–3 are uncorrected line densities. The experimental relative intensities listed in Table II do not agree with the calculated oscillator strengths. The relative intensities of the $2p$-$3d$ lines are nearly constant in the Ne I sequence from Ge to Zr. The intensity ratios of the two $2p$-$3s$ lines change from being nearly equal for Ge to a ratio of about 60% in Zr. The observed intensity ratio for Zr is closer to agreeing with the calculated oscillator strengths of 70% for the $2p$-$3s$ lines in elements Fe through Zr.

The calculated gf values for Ge are approximately equal to the values for Fe XVII that Garstang[14] calculated for the $2p$-$3s$ and $2p$-$3d$ transitions. This Fe ion in the Ne I sequence has been extensively investigated because of its importance in the emission spectrum of the solar corona. Loulergue and Nussbaumer[15] have recently calculated the emission intensities for Ne-like transitions in Fe XVII with a multilevel theory incorporating electron excitation cross sections and cascading effects to arrive at the excited level populations. They find good agreement in the calculated line intensities with recent high-resolution crystal measurements of Fe XVII in a solar spectrum collected by Parkinson.[11] The theory shows that the $3s$ levels are populated mainly by cascading through the $3p$ level. The highest-energy $2p$-$3d$ transition with jj values of $(\frac{1}{2}, \frac{3}{2})$ is almost entirely populated by direct electron excitation from the $2p^6\ {}^1S_0$ ground state. For this reason this $2p$-$3d$ line was selected as reference for tabulating the relative experimental intensity ratios in Table II. The calculated $2p$-$3s$ $(\frac{3}{2}, \frac{1}{2})$ line intensity was nearly equal to the $2p$-$3d$ $(\frac{1}{2}, \frac{3}{2})$ line in Fe XVII, similar to the experimental laser-produced intensities for Ge. The Ge XXIII spectrum, however, does show differences in other line intensities compared to the calculated Fe XVII emission intensities. The relative intensities of both $2s$-$3p$ lines are five times larger and the $2p$-$3d$ $(\frac{3}{2}, \frac{3}{2})$ transition is three times larger in the Ge spectrum than the calculated intensity ratios for Fe XVII. Loulergue and Nussbaumer show that the upper level of the $2p$-$3d$ $(\frac{3}{2}, \frac{3}{2})$ transition is populated largely from the $2s2p^6$ level. Therefore more vacancies are created in the $2s$ inner level

of Ge with plasma excitation than was observed in the Fe XVII solar corona. The relative intensities (50 and 60%) of the $2s$-$3p$ transitions in Ge XXIII are slightly larger than published values of 40 and 50% for Cu XX obtained with the vacuum-spark source at Goddard.[16]

Another difference between solar and laboratory produced spectra is the absence of the magnetic quadrupole transition $2p$-$3s(^3P_2)$ in the laser spectra. The $2p$-$3s(^3P_2)$ magnetic quadrupole transition for which Garstang[17] has calculated its transition probability was found in the high-resolution Fe XVII solar spectrum gathered by Parkinson. There was adequate resolution particularly in the Se spectrum to observe this transition and one can conclude that the metastable $^3P_2$ level is collisionally de-excited in high-density laboratory plasma.

IV. SUMMARY

The laser-produced plasmas combined with crystal spectrographs have been used for atomic spectroscopy in the x-ray energy region to extend the Ne I isoelectronic sequence to $Z = 40$ with a precision comparable to earlier work with grating spectrographs. The ionization stages have been identified in the laser-produced spectra in the region $29 \leq Z \leq 40$. The spectra contain ionization stages that change in a regular manner as one progresses up the Periodic Table. With a laser power of 10–20 J on target, the Zn spectrum consists mainly of Ne, F, and O ionization stages. Weak satellite lines from lower-ionization stages were observed in the Zn and Ge spectra while the satellite structure dominates the Zr spectrum. For an intermediate element such as Se the spectra consist mainly of Ne-like lines. It was not necessary to collect data for every element. The x-ray energies can be interpolated within 2 eV for the missing elements because the square root of the spectral line energies vary linearly for Z above 24 in the Ne I sequence. The atomic-structure calculations for the Na- and Mg-like transitions gave sufficient agreement with the $2p$-$3s$ and $2p$-$3d$ satellite structure to allow interpretation of the Se and Zr spectra. These identifications serve as a prelude to the use of satellites of L-series lines for temperature determinations in medium-Z plasmas.

Note added in proof. A related study of the Ne I transitions in the elements Y–Mo [E. V. Aglitskii *et al.*, Quantum Electron. 1, 2067 (1974)] was brought to our attention after submission of this manuscript. Their experimental values for transitions in Zr XXXI are in good agreement with the values reported here.

---

*Work performed in part under the auspices of the U. S. Atomic Energy Commission.

[1]U. Feldman, G. A. Doschek, D. J. Nagel, R. D. Cowan, and R. R. Whitlock, Astrophys. J. 192, 213 (1974).
[2]P. G. Burkhalter, U. Feldman, and R. D. Cowan, J. Opt. Soc. Am. 64, 1058 (1974).
[3]P. G. Burkhalter, D. J. Nagel, and R. R. Whitlock, Phys. Rev. A 9, 2331 (1974).
[4]B. Edlén and F. Tyrén, Z. Phys. 101, 206 (1936).
[5]F. Tyrén, Z. Phys. 111, 314 (1938).
[6]U. Feldman, L. Cohen, and M. Swartz, Astrophys. J. 148, 585 (1967).
[7]J. M. McMahon and O. C. Barr, in Proceedings of Seventeenth Annual Meeting of the Society of Photo-Optical Instrumentation Engineers, 1973, p. 41 (unpublished).
[8]R. L. Kelly and L. J. Palumbo, *Atomic and Ionic Emission Lines below 2000 Angstroms,* NRL Report No. 7599 (U. S. GPO, Washington, D. C., 1973).
[9]D. J. Nagel *et al.*, Phys. Rev. Lett. 33, 743 (1974).
[10]R. D. Cowan, J. Opt. Soc. Am. 58, 808 (1968).
[11]J. H. Parkinson, Astron. Astrophys. 24, 215 (1973).
[12]U. Feldman and L. Cohen, Astrophys. J. 151, L55 (1968).
[13]U. Feldman and L. Cohen, J. Opt. Soc. Am. 57, 1128 (1967).
[14]R. H. Garstang, Publ. Astron. Soc. Pac. 78, 399 (1966).
[15]M. Loulerque and H. Nussbaumer, Astron. Astrophys. 24, 209 (1973).
[16]M. Swartz, S. Kastner, E. Rothe, and W. Neupert, J. Phys. B 4, 1747 (1971).
[17]R. H. Garstang, Publ. Astron. Soc. Pac. 81, 488 (1969).

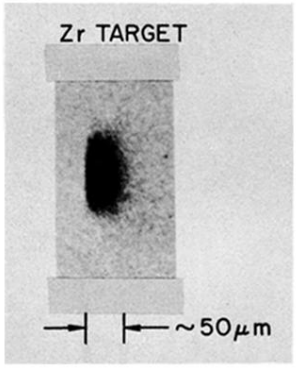

FIG. 5. 1–3-keV x-ray pinhole picture of a Zr target observed at 90° to the laser axis. The laser beam was incident from the right.